

# Case Study: Design, Construction, and Performance of the La Chancelière Parking Garage's Concrete Flat Slabs Reinforced with GFRP Bars

Ehab A. Ahmed, M.ASCE<sup>1</sup>; Brahim Benmokrane<sup>2</sup>; and Maxime Sansfaçon<sup>3</sup>

**Abstract:** Parking garages are among the concrete structures that suffer from corrosion and deterioration due to exposure to deicing salts. The 40-year-old La Chancelière parking garage in Québec (Canada) showed severe corrosion-related deterioration and was in need of costly rehabilitation. As its structural system consisted of two-way flat slabs and the steel reinforcement was severely corroded in most of the slabs, the City of Québec (structure's owner) decided to replace the structure's flat slabs (a total area of about 3,160 m<sup>2</sup>) with new ones, while maintaining the main supporting elements (columns and retaining walls). The consulting firm produced two designs with steel reinforcing bars and glass-fiber-reinforced polymer (GFRP) reinforcing bars. Based on the comparative cost analysis of the steel-reinforced and GFRP-reinforced designs, the city opted for GFRP bars. The flat-slab system was designed according to CAN/CSA S806-12 with GFRP bars as main reinforcement, the world's first application of its type. The slabs were instrumented at critical locations to measure strain with fiber-optic sensors (FOSs) attached to the surface of the GFRP bars or embedded in concrete. This study provides details on the design, construction, and performance of GFRP-reinforced-concrete (GFRP-RC) flat slabs under real service loads and conditions over 3.5 years. In addition, it provides a comparative cost analysis of the steel-RC and GFRP-RC designs. The cost comparison confirms that the initial higher cost of GFRP compared to steel does not necessarily lead to a higher total cost and that a cost-effective design could be achieved. DOI: 10.1061/(ASCE)CC.1943-5614.0000656. © 2016 American Society of Civil Engineers.

**Authors keywords:** Parking garage; Flat slab; Two-way slab; Punching-shear; Design; Glass-fiber-reinforced polymer (GFRP); Fiber-reinforced polymer; Concrete; Monitoring.

## Introduction

Parking garages are exposed to problems related to moisture penetrating the concrete and causing the steel reinforcement to corrode. Extensive use of deicing salts during the winter creates a harsh environment accelerating the corrosion and related deterioration of such structures, possibly leading to catastrophic failures.

Solutions have been proposed to reduce the potential for corrosion and related degradation of parking structures, such as using galvanized-steel bars and epoxy-coated steel bars. The former are restricted in certain countries and the latter are no longer allowed for parking structures under CSA 413 (CSA 2007) due to the debate about the material's durability. On the other hand, replacing corrodible steel reinforcement with noncorroding fiber-reinforced polymer (FRP) bars provides a suitable solution for eliminating the potential of corrosion and the related deterioration. Due to the lower costs of glass FRP (GFRP) compared to the other FRP

types, this material has gained significant attention over the last decade.

Recently, GFRP reinforcement has become a viable solution to eliminate potential corrosion problems in concrete bridge decks (Nanni and Faza 2002; Benmokrane et al. 2006, 2007; Ahmed et al. 2014), bridge barriers (El-Salakawy et al. 2003; Matta and Nanni 2009; Ahmed et al. 2013a, b), and bridge piers (De Luca et al. 2010). On the other hand, limited work has been conducted towards implementing GFRP reinforcement in concrete parking structures.

The Laurier-Taché parking garage in Gatineau, Quebec, Canada (Benmokrane et al. 2004) represents an early implementation of GFRP reinforcing bars in parking-garage structures, in which GFRP reinforcing bars were used as the main reinforcement in the one-way slabs in a demonstration area (about 1,000 m<sup>2</sup>). This successful field implementation of this technology, along with the compelling evidence presented on the durability of GFRP reinforcement in different exposed environments (Mufti et al. 2007), encouraged wider acceptance of this technology in new applications.

A finite-element analysis of two-way flat slab parking-garage structures reinforced with steel, carbon FRP (CFRP), and glass FRP (GFRP) bars was conducted by Razaqpur et al. (1995). This study confirmed the feasibility of replacing steel by either CFRP or GFRP reinforcement for two-way flat slab parking structures if the criteria for acceptability were achievement of flexural strength and deflection control at the serviceability limit state.

With the advancement of FRP technology, a collaborative project between the City of Québec, engineering firms, and the University of Sherbrooke (NSERC Research Chair in Innovative FRP Reinforcement for Concrete Infrastructure) was initiated to implement GFRP reinforcement in parking-garage structures. The first field implementation in a two-way flat-slab parking structure

<sup>1</sup>Postdoctoral Fellow, Dept. of Civil Engineering, Univ. of Sherbrooke, Sherbrooke, QC, Canada J1K 2R1. E-mail: Ehab.Ahmed@USherbrooke.ca

<sup>2</sup>Professor of Civil Engineering, Tier-1 Canada Research Chair in Advanced Composite Materials for Civil Structures and NSERC Research Chair in Innovative FRP Reinforcement for Concrete Structures, Dept. of Civil Engineering, Univ. of Sherbrooke, Sherbrooke, QC, Canada J1K 2R1 (corresponding author). E-mail: Brahim.Benmokrane@USherbrooke.ca

<sup>3</sup>Engineer, EMS Structure Inc., QC, Canada G2J 0B4. E-mail: Maxime.Sansfacon@ems-ing.com

Note. This manuscript was submitted on April 22, 2015; approved on October 20, 2015; published online on March 9, 2016. Discussion period open until August 9, 2016; separate discussions must be submitted for individual papers. This paper is part of the *Journal of Composites for Construction*, © ASCE, ISSN 1090-0268.

was a demonstration area of 350 m<sup>2</sup> reinforced with GFRP bars in the Hôtel de Ville parking garage in Québec (Canada). This demonstration project—in service since 2010—confirmed the feasibility of using GFRP bars in such applications (Ahmed et al. 2011). The behavior of this GFRP-RC section was similar to that of its steel-RC counterparts in the structure. In 2011, the City of Québec commissioned EMS Structure Inc. (Québec, Quebec, Canada) to rehabilitate its La Chancelière parking garage located in the Saint-Roch neighborhood. The contract included examining the options of using either black steel or GFRP bars along with preparing a comparative cost-analysis study for both design options. Based on the designs and the comparative cost analysis provided by the engineering firm, the City opted to use GFRP bars, making this project, to the authors' best knowledge, the world's first of its type.

## Objectives

The authors believe that this paper presents the first innovative flat-slab parking garage reinforced entirely with GFRP reinforcing bars. The study's objectives were to assess the in-service performance of the GFRP-RC flat slabs after years of use; to implement GFRP bars in flat-slab parking garages to eliminate the steel expansive-corrosion issues and related deterioration problems; to design durable and maintenance-free concrete for parking garages; and to demonstrate the use of the GFRP design codes and guideline provisions for designing flat slabs, especially the first punching-shear equation for two-way slabs in the new CSA S806 (CSA 2012) standard. Moreover, the design and construction details of this parking garage are used to illustrate code requirements, flat-slab analysis, design details, and the construction of GFRP-RC flat slabs. In addition, a cost-analysis comparison between steel-RC and GFRP-RC designs is presented.

## Motivation and Cost Analysis

Parking garages are normally subjected to severe exposure conditions that accelerate steel corrosion and shorten their service lives. The design of such structures is often governed by the punching-shear capacity of the slab-column connections. The weakening/deterioration at these connections due to reinforcement corrosion may lead to catastrophic punching-induced failure [such as the case of the parking garage of the Joie de Vivre building in Saint-Laurent, Quebec (Canadian Consulting Engineer 2008)]. Thus, replacing the steel bars with noncorroding FRP reinforcement is expected to yield durable structures with extended service lives. Since GFRP bars are more expensive than steel bars based on a first-cost comparison, there were some concerns about impacts on the project's total cost if GFRP bars were used. Consequently, two designs were produced using steel or GFRP reinforcement to assess the relative costs. The GFRP design was optimized to yield a competitive cost by replacing the garage's waterproofing and asphalt layer with a polyurethane film, which significantly impacted the total cost.

Table 1 presents the detailed comparative cost analysis for both designs. The project's total cost with steel reinforcement was estimated at \$831,400, which includes \$125,000 for steel reinforcement and \$154,000 for flooring (\$70,000 for waterproofing membrane and \$84,000 for the 65-mm asphalt layer). The GFRP design substituted polyurethane membrane for the waterproofing of the entire slab and asphalt layer, which reduced the project's total cost by \$85,800, making the estimated cost for the GFRP design \$794,450. Consequently, even though the GFRP design incurred higher material costs than the one with black steel, the total cost of the structure reinforced with GFRP was surprisingly lower

**Table 1.** Comparative Cost Analysis between GFRP and Black-Steel Bars

Description	Steel		GFRP	
	Quantity	Total	Quantity	Total
Mobilization and demolition	1 lot	\$10,000	1 lot	\$10,000
Demolition of concrete	650 m <sup>3</sup>	\$162,500	650 m <sup>3</sup>	\$162,500
Preparing the surface				
Polishing the slabs	2,800 m <sup>2</sup>	\$2,800	2,800 m <sup>2</sup>	\$2,800
Curing for 7 days	2,800 m <sup>2</sup>	\$2,100	2,800 m <sup>2</sup>	\$2,100
Formwork				
Structural slabs	2,800 m <sup>2</sup>	\$140,000	2,800 m <sup>2</sup>	\$140,000
Drop panels	60 units	\$9,000	60 units	\$9,000
Ramps	100 m <sup>2</sup>	\$8,500	100 m <sup>2</sup>	\$8,500
Reinforcement				
10M to 35M steel <sup>a</sup>	50,000 kg	\$125,000	—	—
20M to 35M GFRP <sup>b</sup>	—	—	42,160 m	\$210,800
Concrete				
30 MPa + casting	740 m <sup>3</sup>	\$106,500	740 m <sup>3</sup>	\$106,500
Links to existing concrete				
Wall—slab	310 m	\$31,000	310 m	\$31,000
Column—slab	40 units	\$80,000	40 units	\$80,000
Covering (flooring)				
Waterproofing membranes	2,800 m <sup>2</sup>	\$70,000	—	—
Asphalt—65 mm	2,800 m <sup>2</sup>	\$84,000	—	—
Membrane—columns (base)	—	—	40 units	\$8,000
Membrane—walls (perimeter)	—	—	310 m	\$23,250
Total cost	—	\$831,400	—	\$794,450

<sup>a</sup>Steel bars with a yield strength not less than 400 MPa.

<sup>b</sup>GFRP bars with a modulus of elasticity not less than 60 GPa.

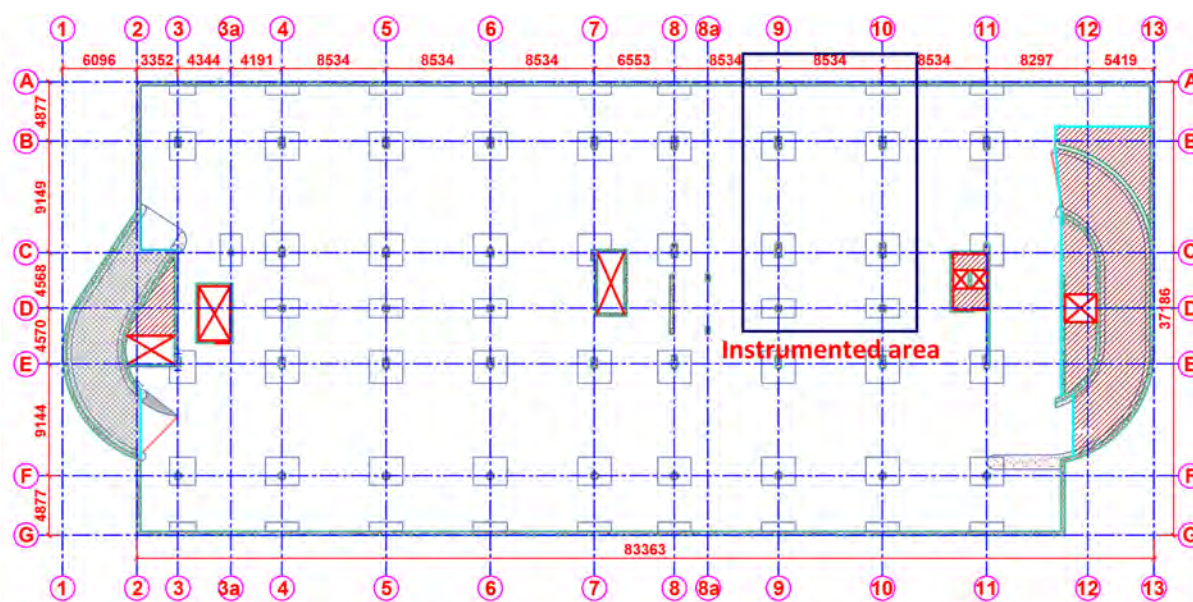
(\$794,450 with GFRP compared to \$831,400 with steel). Thus, the initial cost of the GFRP materials may not be a problem since, in some cases such as parking garages, the total cost of a GFRP-reinforced structure can be controlled so as to be relatively close to that of a steel-reinforced structure. Furthermore, the estimated construction time for the construction with GFRP bars was estimated at 6,860 h compared to 7,700 h in the case of steel bars, which provides another advantage when GFRP bars are used.

## Project Description

La Chancelière parking garage—located on Du Roi Street in the Saint-Roch neighborhood of Québec (Quebec, Canada)—is a 40-year-old, two-story (levels A, B) reinforced-concrete (RC) structure under a multistory residential building, as shown in Fig. 1(a). The garage is 83.36 m long and 37.86 m wide, for a total area of about 3,160 m<sup>2</sup>. The garage's original structural system was a two-way flat slab supported on columns and retaining walls. The slab thickness was 230 mm, increasing to 367 mm over the columns (drop-panel area). The slabs were built with a clear concrete cover of about 25 mm. Recently, the La Chancelière parking garage showed severe deterioration directly resulting from the corrosion of steel reinforcement and the consequent spalling of the concrete cover as shown in Fig. 1(b). This led to faster degradation and reduction in the cross-sectional area of the steel reinforcement. This deterioration led to the need to undertake a costly rehabilitation of the slabs on level A. Since two-way slabs were used and the steel reinforcement was very severely corroded in most of the slabs, it was then decided to replace the entire slabs on level A while preserving the main supporting elements (columns and retaining walls), which could be repaired later, as needed. Fig. 2 shows the layout of the La Chancelière parking garage. In Fig. 2, the circled numbers (1–13) refer to the transverse axis, while the circled letters



**Fig. 1.** La Chancelière (images by Ehab A. Ahmed): (a) photo of the residential building; (b) corrosion of steel reinforcement in a slab



**Notes:**

Circled numbers (1 to 13) refer to transverse axis while circled letters (A to G) refer to the longitudinal axis. Dimensions are in mm.

**Fig. 2.** Layout of the La Chancelière parking garage

(A to G) refer to the longitudinal axis. GFRP reinforcing bars were used in the new structural flat slabs to eliminate the potential for corrosion and provide a maintenance-free structure with an extended service life.

### Material Properties

This project involved a single grade of sand-coated GFRP bars: grade III, as classified in CSA S807 (CSA 2010) according to Young's modulus (60 GPa) in four designated diameters: #15, #22, #25, and #32 [with nominal cross-sectional areas of 199, 387, 510, and 819 mm<sup>2</sup>, respectively, as indicated in CSA (2010)]. The immersed cross-sectional areas of these bars were also determined through testing and were 273, 540, 702, and 1,028 mm<sup>2</sup> for #15, #22, #25, and #32 GFRP bars, respectively. It can be noticed

that the immersed (measured) cross-sectional areas of the used GFRP bars were higher than the nominal cross-sectional areas. Table 2 summarizes the mechanical properties of the GFRP bars, as provided by the manufacturer (Pultrall, Thetford Mines, Quebec). It should be mentioned that about 40,000 longitudinal meters were used in this project, which included 1,240 m of #15, 37,883 m of #22, 158 m of #25, and 513 m of #32 GFRP bars.

The slabs were designed and constructed with type E-1 concrete with a nominal compressive strength of 35 MPa. Table 3 provides the concrete mix proportions. A total of 740 m<sup>3</sup> of concrete was used to build the structural flat slabs.

### Design of the Parking-Garage Flat Slabs

The total thickness of the new slabs (base thickness + drop panel = 367 mm) was maintained as the original slabs to preserve the clear

**Table 2.** Tensile Properties of the GFRP Bars Used in the Flat Slabs (Data from Pultrall 2011)

Designation of GFRP bars <sup>a</sup>	Nominal cross-sectional area <sup>a</sup> (mm <sup>2</sup> )	Immersed cross-sectional area (mm <sup>2</sup> )	Tensile strength <sup>b</sup> (MPa) average ± standard deviation	Tensile modulus of elasticity <sup>b</sup> (GPa) average ± standard deviation	Average strain at ultimate <sup>b</sup> (%)
#15	199	273	1,323 ± 12	64.8 ± 0.5	2.0
#22	387	540	1,405 ± 37	70.6 ± 0.4	2.0
#25	510	702	1,113 ± 14	66.9 ± 0.4	1.6
#32	819	1,028	1,149 ± 11	76.3 ± 1.0	1.5

<sup>a</sup>According to CSA S807 (CSA 2010).

<sup>b</sup>Tensile properties were calculated using nominal cross-sectional areas.

**Table 3.** Concrete Mixture Proportions

Property	Value
Concrete type	E-1
Nominal concrete strength (MPa)	35
Slump (mm)	82 ± 19
Air entrained (%)	5–8
Maximum aggregate size (mm)	19
Cement type	10SF

height in the garage. The flat slabs were slightly thicker (260 mm) than the original one (230 mm) to achieve a sufficient fire rating. The additional dead load was minimal relative to the total loads on the existing columns. The design was made according to *Parking Structures* (CSA 2007); *Design and Construction of Building Components with Fiber-Reinforced Polymers* (CSA 2012); and *Design of Concrete Structures* (CSA 2004). The loads were calculated according to the *National Building Code of Canada* (NBCC 2005). The design was conducted using the nominal cross-sectional areas of the GFRP bars according to the *Specification for Fiber-Reinforced Polymers* (CSA 2010). This section summarizes the design of parking-garage flat slabs.

### Design for Fire Endurance

One of the critical design issues for parking garages is the fire endurance. According to CSA (2012), fire endurance is controlled by the concrete cover, and typical design charts are provided based on the work of Kodur and Baingo (1998). Using the fire endurance charts in Annex R *Procedure for the determination of a fire-resistance rating for concretes labs reinforced with FRP and concrete members strengthened with FRP* in CSA (2012), the concretes labs were designed for a 2-h fire endurance with a clear concrete cover of 60 mm.

### Structural Analysis of the Parking Garage

The structural analysis of the parking garage was conducted using a commercial finite-element (FE) software (SAFE Software 2011), assuming the loads in accordance with the NBCC (2005) where the dead load was 6.15 kPa and the live load was 2.4 kPa. The bending moments for the column strips and field strips in both directions were determined from the FE analysis. Two different load combinations were used in the analysis for the ultimate limit state and serviceability limit state. Fig. 3 shows a typical structural analysis of the parking garage with SAFE Software (2011); the bending moments of the slab system in one direction ( $M_{11}$ ) are presented at service (dead load +live load) and at factored load (1.25 dead load + 1.50 live load). It should be mentioned that the bending moments of column strips and field strips can be seen from the distribution of the moments in Fig. 3.

### Flexural Design for Ultimate Strength

The thickness of the new flat slabs reinforced with GFRP bars was adjusted (+25 mm) for the fire-resistance rating. The slab thickness at the columns were increased using drop panels to resist the combined flexural and punching-shear stresses. The slab base thickness in the areas between the columns was 260 mm (increased from 230 mm with respect to the original steel-reinforced ones to for fire endurance), while the areas above the columns (drop-panel area) were increased to 367 mm in thickness (to maintain clear height). The concrete cover resulting from the fire-endurance design was 60 mm, which satisfies the minimum concrete cover requirements in CSA (2012) of  $2d_b$  or 30 mm.

The flexural design was based on the strain compatibility assumptions specified in CSA (2012), in which the strain in the reinforcement and concrete is assumed to be directly proportional to the distance from the neutral axis. At the ultimate limit state, the flat-slab sections were designed so that section failure would be initiated by crushing of the concrete in the compression zone (over-reinforced section) as specified in CSA (2012) according to the following equation:

$$\frac{c}{d} > \frac{7}{7 + 2,000\varepsilon_f} \quad (1)$$

Once Eq. (1) had been satisfied, the distribution of the concrete stress over the cross section was defined as follows:

1. A concrete stress of  $\alpha_1\phi_c f'_c$  is assumed to be uniformly distributed over an equivalent compression zone bounded by edges of the cross-section and a straight line located parallel to the neutral axis at a distance  $a = \beta_1 c$  from the fiber of maximum compressive strain (the distance  $c$  is measured in a direction perpendicular to that axis); and
2. The factors  $\alpha_1$  and  $\beta_1$  shall be calculated as

$$\beta_1 = 0.97 - 0.0025f'_c \geq 0.67 \quad (2a)$$

$$\alpha_1 = 0.85 - 0.0015f'_c \geq 0.67 \quad (2b)$$

Employing strain compatibility and using the uniformly distributed stress block for concrete, the compressive and tensile forces resisted by the concrete and GFRP reinforcement can be determined as follows, respectively:

$$C = \alpha_1\phi_c f'_c b a = \alpha_1\phi_c f'_c b (\beta_1 c) \quad (3)$$

$$T = \phi_f \varepsilon_f E_f A_f = \phi_f \left[ \frac{\varepsilon_c}{c} (d - c) \right] A_f \quad (4)$$

Through equating the compressive [Eq. (3)] and tensile [Eq. (4)] forces, the value of the neutral-axis depth ( $c$ ) was determined. The

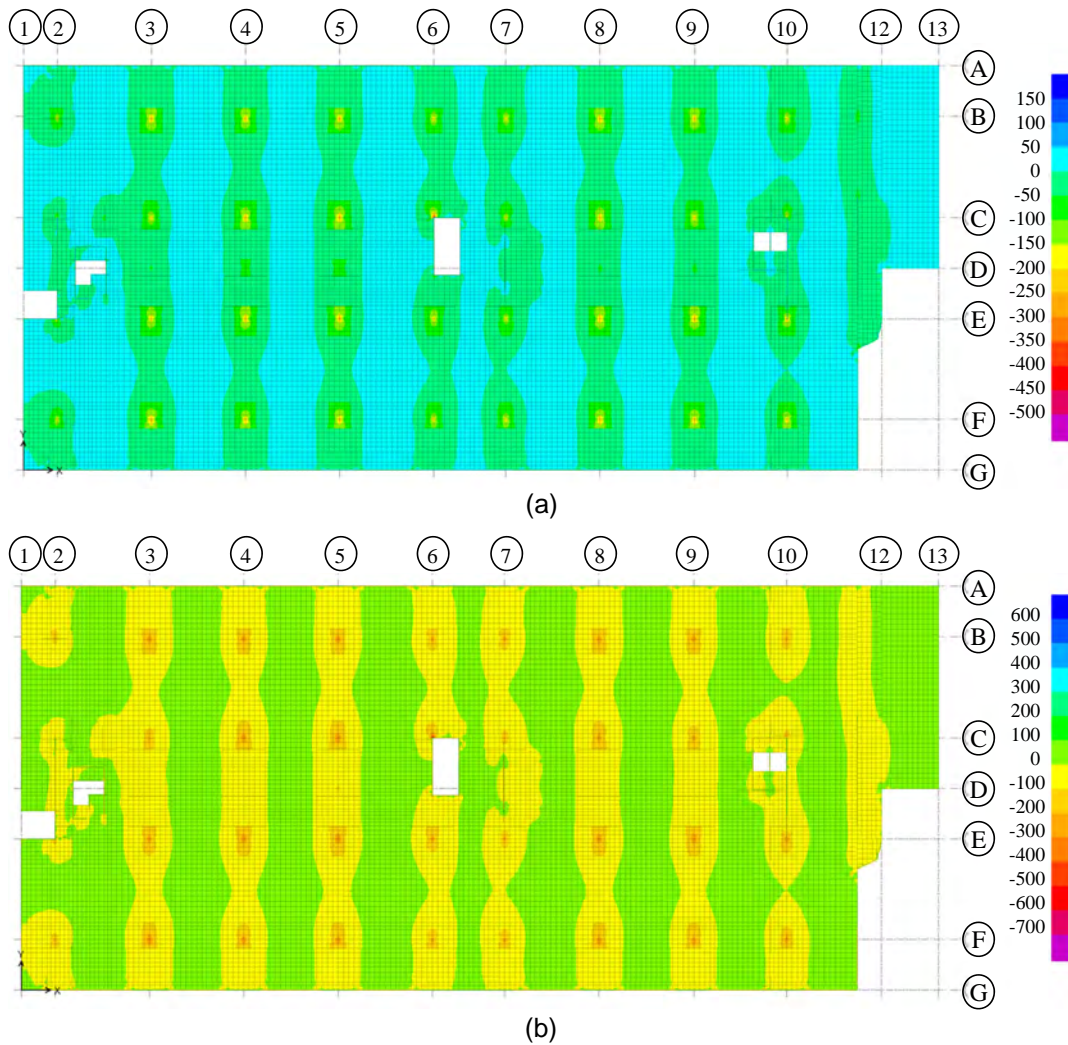


**Fig. 3.** Analysis of the slabs using SAFE software: (a) slab resultant moment  $M_{11}$  in  $\text{kN} \cdot \text{m}/\text{m}$  for the service load (dead load + live load); (b) slab resultant moment  $M_{11}$  in  $\text{kN} \cdot \text{m}/\text{m}$  for the factored load (1.25 dead load + 1.50 live load)

ultimate strain at the extreme concrete compression fiber ( $\epsilon_c$ ) was assumed to be 0.0035 and the material resistance factor for GFRP bars ( $\phi_f$ ) was taken as 0.75 and the material safety factor for concrete ( $\phi_c$ ) was taken as 0.65. The design satisfied the requirement that the factored moment resistance ( $M_r$ ) was greater than or equal to factored applied moment ( $M_f$ ). The minimum reinforcement was also verified, where  $M_r > 1.5M_{cr}$ , where  $M_{cr}$  is calculated using the modulus of rupture,  $f_r = 0.6\sqrt{f'_c}$ . In addition, the minimum area of reinforcement of  $400/E_f A_g \geq 0.0025A_g$  with a spacing no farther apart than three times the slab thickness or 300 mm, whichever is less, was verified.

The flexural design of the slabs yielded #22 GFRP spaced at 140 mm in the negative moment area (over columns) and #22 GFRP spaced at 200 mm in the positive moment areas (between columns) for the column strip. In addition, it yielded #22 GFRP spaced at 300 mm and #22 GFRP spaced at 230 mm for the negative and positive moment areas in the field strip, respectively. The Appendix provides a typical design example.

#### **Flexural Design for Serviceability (Crack Width, Stress at Service, and Deflection)**

According to CSA (2012), when the maximum strain in FRP tension reinforcement under full service loads exceeds 0.0015 (1,500

microstrains), the crack width should be checked and verified against the permissible limits using a crack-control parameter,  $z$ , which is calculated as shown in Eq. (5). The cross-sections of maximum positive and negative moment must have a  $z$  value not exceeding 45,000  $\text{N}/\text{mm}$  for interior exposure and 38,000  $\text{N}/\text{mm}$  for exterior exposure. It should be mentioned that these values for parameter  $z$  correspond to limiting crack widths to 0.7 mm (interior exposure) and 0.5 mm (exterior exposure), respectively

$$z = k_b \frac{E_s}{E_f} f_{fSLS} \sqrt[3]{d_c A} \quad (5a)$$

$$k = \sqrt{2\rho_f n_f + (\rho_f n_f)^2} - \rho_f n_f \quad (5b)$$

$$n_f = E_f / E_c \quad (5c)$$

$$E_c = (3,000\sqrt{f'_c} + 6,900)(\gamma_c/2,300)^{1.5} \quad (5d)$$

$$f_{fSLS} = \frac{M_{SLS}}{A_f d \left(1 - \frac{k}{3}\right)} < 0.25 f_{FRPu} \quad (5e)$$

In calculating  $d_c$  and  $A$  in Eq. (5a), the effective clear cover need not be taken as greater than 50 mm. The bond-dependent coefficient,  $k_b$ , used in the calculations in Eq. (5a) was 0.8 for sand-coated GFRP bars. It should be mentioned that the modulus of elasticity of concrete [Eq. (5d)] was provided in CSA (2004). The design of the slabs was based on the severe exposure condition and the crack control parameter,  $z$ , was less than 38,000 N/mm.

The stress level in the GFRP reinforcing bars at serviceability limit state, calculated from Eq. (5e), should not exceed 0.25 of the characteristic tensile strength (average tensile strength-3 × standard deviation). The Appendix provides a typical design example.

The deflection at service load was calculated using the ACI 440 Committee (ACI 440-H) expression for  $I_e$  that works for both FRP- and steel-RC members without the need for empirical correction factors (Bischoff and Scanlon 2007). The expression, presented in Eq. (6), included the new factor ( $\gamma$ ), which accounts for stiffness variation along the member. The calculated deflection satisfied the requirements in CSA (2004)

$$I_e = I_{cr}/[1 - \eta\gamma(M_{cr}/M_a)^2] \leq I_g \quad (6a)$$

$$\eta = 1 - (I_{cr}/I_g) \quad (6b)$$

$$\gamma = 1.72 - 0.72(M_{cr}/M_a) \quad (6c)$$

### Design for Punching-Shear Strength

The punching-shear strength,  $V_c$ , of the slabs was calculated according to CSA (2012), where  $V_c$  is the smallest of the following:

$$V_c = 0.028\lambda\phi_c \left(1 + \frac{2}{\beta_c}\right) (E_f\rho_f f'_c)^{1/3} b_{o,0.5d} d \quad (7a)$$

$$V_c = 0.147\lambda\phi_c \left(\frac{\alpha_s d}{b_{o,0.5d}} + 0.19\right) (E_f\rho_f f'_c)^{1/3} b_{o,0.5d} d \quad (7b)$$

$$V_c = 0.056\lambda\phi_c (E_f\rho_f f'_c)^{1/3} b_{o,0.5d} d \quad (7c)$$

where  $\beta_c$  = ratio of the long side to short side of the column, concentrated load, or reaction area; and  $\alpha_s = 4$  for interior columns, 3 for edge columns, and 2 for corner columns. The concrete strength in Eq. (7) should be less than 60 MPa. If the effective depth of the structural slab exceeds 300 mm,  $V_c$  shall be multiplied by  $(300/d)^{0.25}$ . It should be mentioned that Eq. (7c) generally controls the capacity in the case of square columns or columns with a  $\beta_c$  close to 1.

### Development and Splice Lengths

The development lengths ( $l_d$ ) of the GFRP bars in tension was determined according to CSA (2012) using Eq. (8)

$$l_d = 1.15 \frac{k_1 k_2 k_3 k_4 k_5}{d_{cs}} \frac{f_f}{\sqrt{f'_c}} A_b \quad (8)$$

where  $d_{cs}$  shall not be taken greater than  $2.5d_b$  and  $\sqrt{f'_c} < 5$  MPa.

The former equation confirms that the development length is dependent on GFRP bar diameter ( $d_b$ ), the design stress in GFRP tension reinforcement at the ultimate limit state ( $f_f$ ), and the concrete compressive strength ( $f'_c$ ). This length is also governed by five other factors, namely, the bar-location factor ( $k_1$ ), concrete-density factor ( $k_2$ ), bar-size factor ( $k_3$ ), bar-fiber factor ( $k_4$ ), and

bar-surface profile factor ( $k_5$ ). In the calculations, the corresponding values for these factors were taken as  $k_1 = 1.3$  or 1.0 (top or bottom bars),  $k_2 = 1.0$ ,  $k_3 = 0.8$  or 1.0 (area < 300 mm<sup>2</sup> or area > 300 mm<sup>2</sup>),  $k_4 = 1.0$ , and  $k_5 = 1.0$ . In addition, the splice length was set to 1.3  $l_d$ . It should be mentioned that the development length of the top bars was increased by 30% with respect to the bottom bars to account for the top-bar effect, which can be verified from  $k_1$  values (1.3 and 1.0 for top and bottom bars, respectively).

### Construction of the Parking Garage

The demolition and reconstruction of the flat slabs was divided into three stages. Stage 1 included the area between axes 1 and 5. Stage 2 included the adjacent section up to axis 8a, while the remaining area was constructed as the last stage (Stage 3). During the demolition, the slabs were totally removed and a steel bracing system was provided to protect the columns and the retaining wall against excessive buckling. Fig. 4 shows the demolition and reconstruction stages; the bracing system is also illustrated. The construction started in March 2011 and was completed in October 2011; the facility opened in November 2011.

Once the slab had been demolished in each stage, the formwork was prepared and the GFRP reinforcement installed, as shown in Fig. 5. The slabs were reinforced with Grade III #22 GFRP bars (CSA 2010). Slab continuity with the existing supporting elements (columns and retaining walls) was achieved by anchoring the #22, #25, and #32 GFRP bars in drilled holes using rotary pits and an adhesive (Hilti Canada 2011), as shown in Fig. 6. Since the immersed (measured) cross-sectional areas of the used GFRP bars were higher than the nominal cross section areas, the contractor considered drilling the holes with diameters suitable for accommodating the actual GFRP bars. In addition, galvanized-steel corbels were used to anchor the slab to the column to provide additional safety for the connections.

It should be mentioned that the instrumentation for monitoring the strains in the GFRP bars and concrete was used in the flat slabs cast in Stage 3. The bars were delivered instrumented to the construction site and were installed in the desired locations; their cables were assembled and connected to the data-acquisition systems before casting. The concrete in this stage was cast on August 10, 2011 (Fig. 7).

Since there had been no similar applications in which flat slabs had been cast with existing columns and continuity (wall-slab and column-slab) achieved with grouted anchors, galvanized-steel corbels were used to provide additional punching protection for the slabs at the columns and walls, as shown in Figs. 8(a and b). The galvanized-steel corbels were attached to the columns and the retaining walls after the formwork was removed, serving as heads to reduce the punching-shear stresses around the columns and provide additional safety to the connection. Nonshrink grout was then used between the steel plates and slabs.

Furthermore, in order to cast the slabs, the concrete cover of the columns had to be removed and adhesive anchors for slab reinforcement had to be installed. As a result, the columns needed rehabilitation. This was also performed because the columns showed some signs of deterioration in the concrete cover close to the slab surface. Column rehabilitation extended approximately 400 mm measured from the slab surface. The concrete cover was sawn and removed with a pneumatic drill, as shown in Fig. 9(a), before new concrete was cast. The retaining walls were also repaired where needed. The steel reinforcement of the columns showed no signs of significant deterioration; there was no need to replace or add any additional reinforcement. The dimensions



**Fig. 4.** Demolition and construction (images by Ehab A. Ahmed): (a) Stage I (Axes 1 to 5); (b) Stage II (Axes 6 to 8a)



**Fig. 5.** Placement of GFRP reinforcement (image by Ehab A. Ahmed)

of the column bases were increased by 75 mm in each direction in order to pour the concrete. Fig. 9(b) shows a typical supporting column after rehabilitation.

Although the new slabs were reinforced with noncorrodible GFRP bars, a concrete surface coating was needed to provide protection and prevent water, salt, and chemicals from penetrating the concrete slabs or the supporting columns and walls. An asphalt layer has conventionally been used for this purpose in many parking garages. In this project, however, a thin layer of polyurethane was used on the slabs and columns for protection. This material is characterized by resistance to water, chemicals, scratching, and abrasion (which is necessary for parking facilities), and stability under ultraviolet exposure, which means it will not yellow like epoxy does when exposed to small amounts of sunlight over periods of time (close to entrances). In addition, using a polyurethane layer reduced the dead load resulting from the asphalt layer, thereby having a positive impact on the design. Furthermore, substituting the asphalt layer with a polyurethane layer significantly contributed to the price difference between the GFRP and steel designs, thereby confirming that cost-effective designs with GFRP bars could be achieved by considering the circumstances of each structure. Fig. 10 shows the parking garage in service once rehabilitation had been and the membrane layer installed.

### Instrumentation with Fiber-Optic Sensors

A representative area of the parking garage (Fig. 2) was selected for monitoring the behavior and assessing the performance of the GFRP-RC flat slabs. The GFRP reinforcing bars and the concrete section of the slab were instrumented at critical locations collect strain data with fiber-optic sensors (FOSs). The instrumented GFRP bars were transported to the construction site for storage until installation. The FOSs were glued to bottom and top reinforcing bars in the two orthogonal directions at the location of the maximum expected stresses. In addition, two FOSs were glued to two dummy bars embedded in the flat slab inside a PVC tube, so that the effects of temperature variation on the strain readings could be recorded. The compressive concrete strain at the midspan was also captured using two FOSs embedded in the concrete. Fig. 11 shows the instrumentation of the GFRP bars and concrete sections, while Fig. 12 shows the locations and identifications of the FOSs and the two readout units.

The FOSs were controlled by two 16-channel data-acquisition systems (Fig. 12) for long-term monitoring and structural-performance assessment. For the moment, there are no phone lines connected to the data loggers. Arrangements as being considered for a permanent location and phone line connection to facilitate data collection. The FOSs and data loggers allow for the long-term monitoring and field assessment of the behavior of two-way flat slabs reinforced with GFRP bars under real service loading and environmental conditions.

Before the FOSs were installed in the field, two representative sensors were glued to GFRP bars from the same production lot and tested in tension on a test machine to verify the glue's performance and effectiveness at high strain levels. The test yielded a linear relationship between the stress in the GFRP bar and the corresponding strain measured by the FOS up to a strain of 3,700 microstrains. Consequently, the test confirmed the performance of the sensor and the glue, indicating that the FOS was capable of withstanding a high strain level (up to 3,700 microstrains) without any problems.

### General Performance and Monitoring Results

To date, the parking garage is performing structurally as expected, with no special issues or problems. Periodic visits were made to the parking to check the overall performance through a visual inspection and to collect the readings of the FOSs. The last visit was made on April 10, 2015 (3.5 years in service). The readings of the FOSs, however, were collected and reported until December 13, 2013



**Fig. 6.** Installation of the anchors in walls and columns (images by Ehab A. Ahmed): (a) drilling the holes in columns; (b) drilling the holes in walls; (c) installing the GFRP bars in columns; (d) installing the GFRP bars in walls



**Fig. 7.** Concrete casting (images by Ehab A. Ahmed)

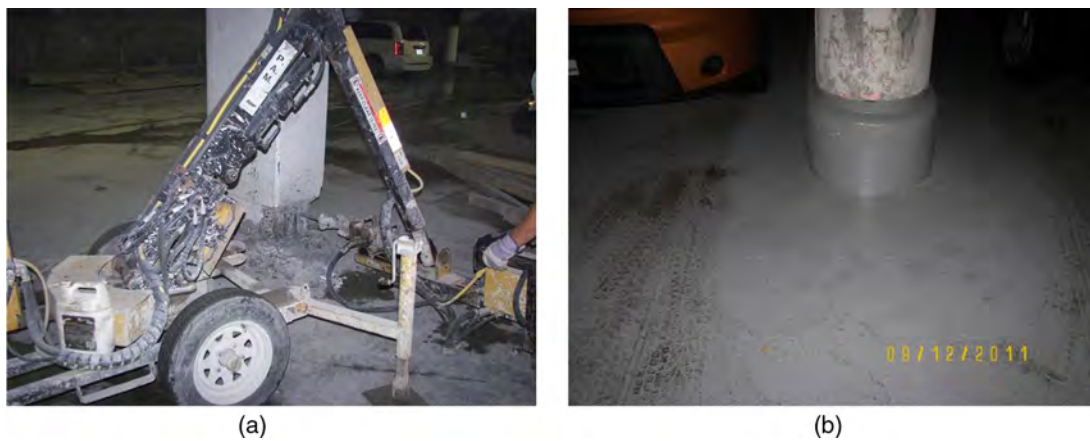
because the time-strain relationships were stabilized. The new slabs exhibited flexural cracks similar to those normally observed in such structures. Since there has been no continuous monitoring or mapping of the cracks, the strain measured by the FOSs have been used to assess the garage's structural performance.

Fig. 13 shows the total strain in the top and bottom GFRP bars at critical sections, while Fig. 14 shows the strains in the dummy bars. The concrete strains are presented in Fig. 15. It should be mentioned that the effect of the temperature variation on the strain variation in the top and bottom GFRP bars is included in the strain

measurements presented in Fig. 13. The identification of the FOSs were introduced on Figs. 13–15, while the locations of the FOSs can be verified from Fig. 12. The initial readings for the strains were recorded on August 9, 2011 at 8:00 p.m. (a few hours before casting). Thus, the reported strain values included concrete shrinkage. Besides, the effect of the high temperature due to cement hydration at the early age of concrete on the strain measurements can be captured. The sudden strain variation due to the dead load after formwork removal can be also seen in the strains in the bottom and top GFRP bars and the concrete.



**Fig. 8.** Steel corbels (images by Ehab A. Ahmed): (a) around columns; (b) along walls



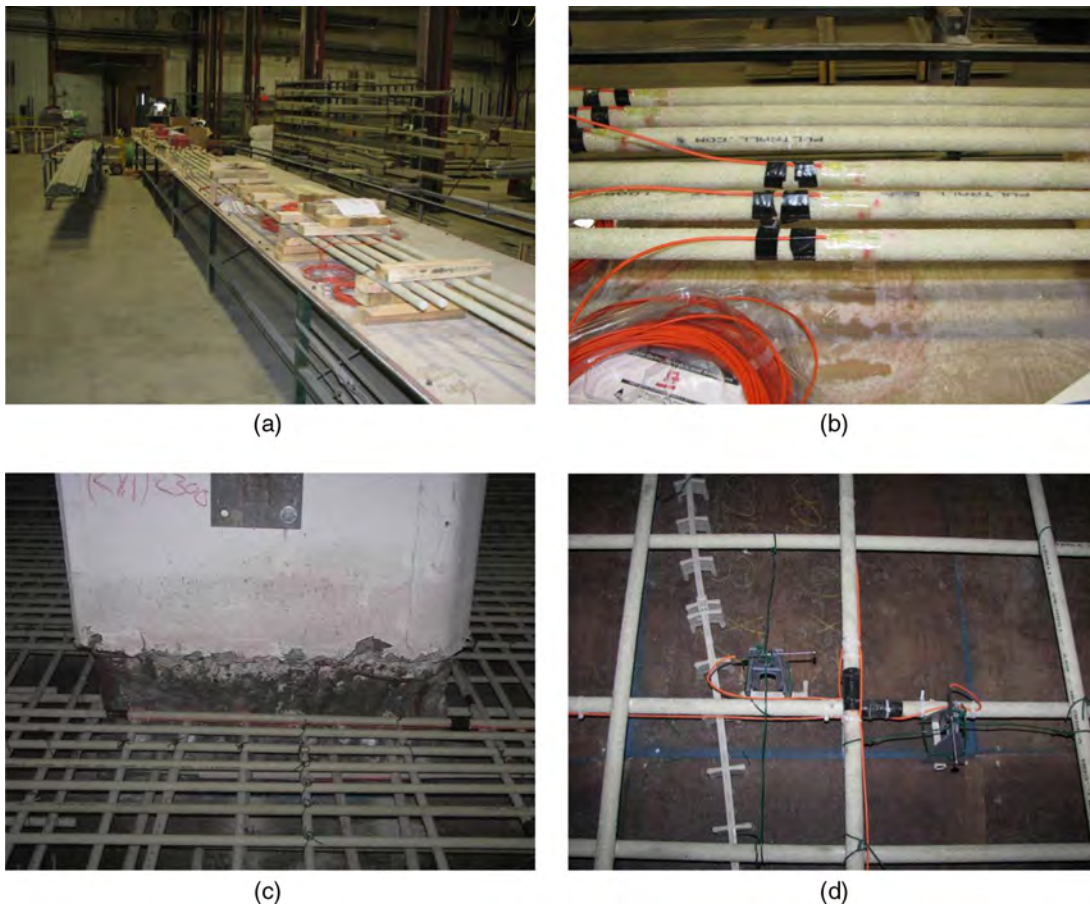
**Fig. 9.** Rehabilitation of columns (images by Ehab A. Ahmed): (a) removing the concrete cover; (b) column section after rehabilitation



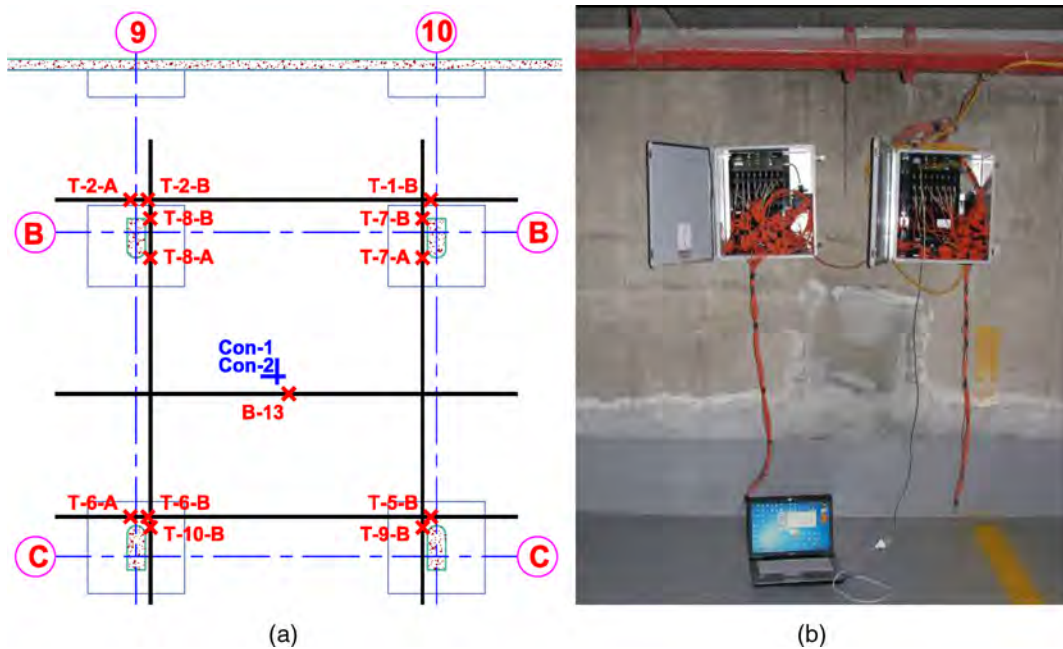
**Fig. 10.** Parking garage in service (image by Ehab A. Ahmed)

Fig. 13(a) reveals a sharp increase of about 2,000 microstrains in the bottom GFRP bars when the formwork was removed. After that, the strain increased to about 2,500 microstrains when the parking garage was opened to the public. The 2,500 microstrains

represent about 15% of the strain capacity of the #22 GFRP bars used. It has stabilized at about 2,750 microstrains. Similar behavior was observed in the top reinforcing bars, but the maximum strain was about 1,450 microstrains, as shown in Fig. 13(b), which represents 8% of the strain capacity of the GFRP bars. In the case of most flat slabs, the negative bending moments in the column area are higher than those at mid-span. The results, however, indicate that measured strains in the top GFRP reinforcing bars in the negative moment area were smaller than those measured in the GFRP bars at midspan. The maximum design stress in the GFRP bars located at the columns at service state was 199 MPa (corresponding to a strain of 3,000 microstrains as the design was made using a modulus of elasticity equal to 65.5 GPa), while the measured strain was about 1,450 microstrains. On the other hand, the maximum stress in the midspan at service state was 126 MPa (corresponding to a strain of 1,923 microstrains), while the measured strain was about 2,750 microstrains. Since the slabs were not cast monolithically with the columns, the negative moment was redistributed due to cracking and the change in the flexural stiffness and the effective value was different from those used in the design. Consequently, the measured strains in the negative moment area were lower than those obtained from the design ( $1,450/3,000 \times 100 = 48\%$ ), while the strains in the positive moment were higher than those obtained from the design ( $2,750/1,920 = 143\%$ ). Assuming that the bending moments are directly proportional to the measured strains, the



**Fig. 11.** FOS instrumentation (images by Ehab A. Ahmed): (a) preparing the GFRP bars; (b) FOSs glued to the GFRP bars; (c) instrumented GFRP bars at desired locations; (d) concrete FOSs



**Fig. 12.** Locations of the FOSs and data loggers (image by Ehab A. Ahmed): (a) identification of the various sensors; (b) readout units

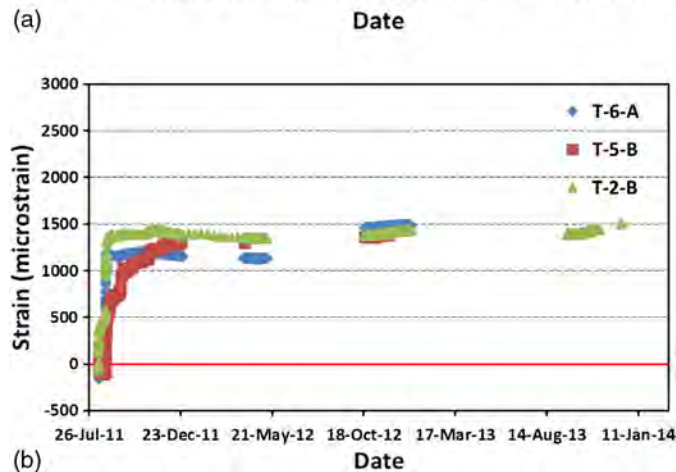
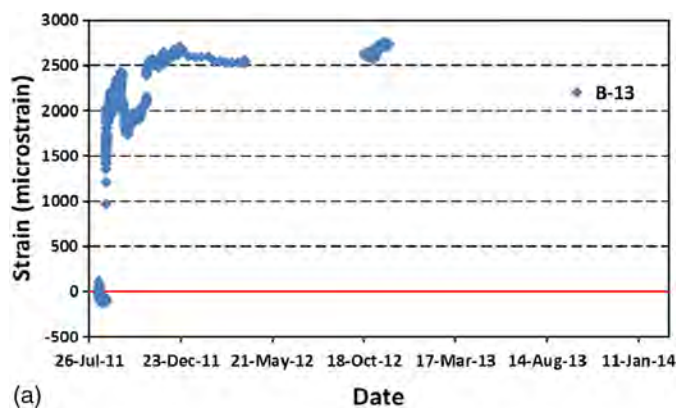


**Fig. 13.** Measured reinforcement strains: (a) bottom GFRP bars; (b) top GFRP bars

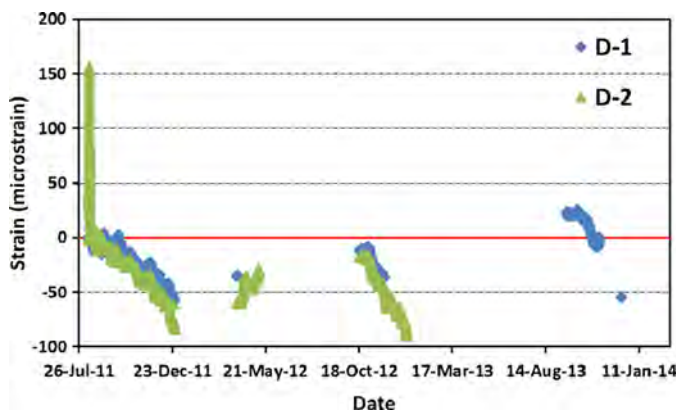


**Fig. 14.** Measured strains in the dummy bars

measured strains confirm that the reduction in the negative moment (redistribution), which is 48%, is very close to the increase in the positive moment, which is 43%. Thus, when designing flat slabs that are not cast monolithically with the supporting columns, the positive moment sections should be designed to resist additional moments due to the redistribution of the negative moments at the columns. El-Mogy et al. (2010) reported similar moment redistribution for continuous concrete beams reinforced with GFRP bars; however, tests are yet to be conducted on the continuous two-way flat slabs.

On the other hand, Fig. 14 indicates that the two dummy bars showed a strain increase of about 150 microstrains due to the hydration temperature after casting. After that, their strain readings

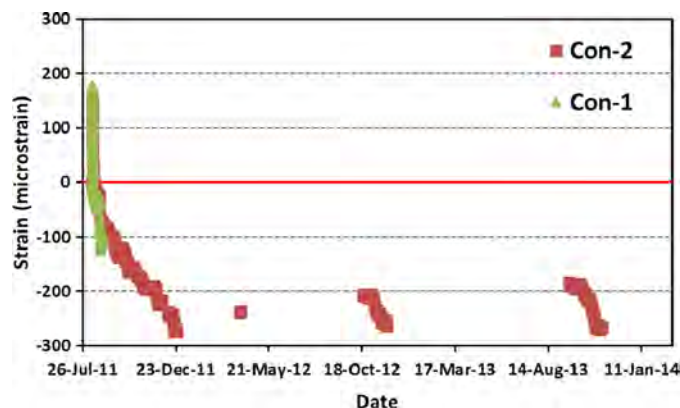


**Fig. 15.** Measured concrete strains

changed slightly due to the seasonal variation in temperature inside the parking garage. As mentioned earlier, the effect of the temperature variation on the strain variation in the top and bottom GFRP bars is included in the strain measurements presented in Fig. 13.

The concrete strain presented in Fig. 15 shows the early-age strain variation resulting from hydration and shrinkage. A sudden increase of about  $-125$  microstrains was recorded due to the dead load when the formwork was removed. The maximum recorded concrete strain was about  $-300$  microstrains. Besides, Fig. 15 indicates that the strains stabilized and that a slight variation in the compressive-strain values followed the seasonal temperature variation inside the parking garage.

## Summary and Conclusions

This paper presented the design, construction, and monitoring of the structural GFRP-reinforced-concrete flat slabs of the La Chancelière parking garage in Québec (Quebec, Canada), which is, to the authors' best knowledge, the first innovative flat-slab parking garage reinforced totally with GFRP reinforcing bars. Based on the results and discussion presented herein, the following conclusions can be drawn:

- The GFRP bars provided a viable and cost-effective solution to overcome corrosion issues in a reinforced concrete parking garage structure. The new slabs were designed using the same concrete sections as the original slabs, making it possible to preserve the clear height and the loads resulting from self-weight.
- The CSA (2012) design provisions used in designing the flat slabs led to an adequate design that satisfied the serviceability and strength criteria.
- No obstacles to construction were encountered as the result of using the GFRP bars in the flat slabs. The GFRP bars withstood normal on-site handling and concrete placement with no problems. The GFRP adhesive anchors to ensure continuity in the columns and slabs were also installed without incident. The holes were drilled with diameters suitable for accommodating the actual GFRP bars since the immersed (measured) cross-sectional areas of the used GFRP bars were higher than the nominal cross section.
- The GFRP-RC flat slabs showed normal structural performance in terms of strain and cracking throughout 3.5 years of real service conditions. The maximum measured strains in the GFRP bars did not exceed 20% of their strain capacity, but were lower than the expected strains.
- The midspan sections in flat slabs should be designed so as to resist the bending moments resulting from the redistributed

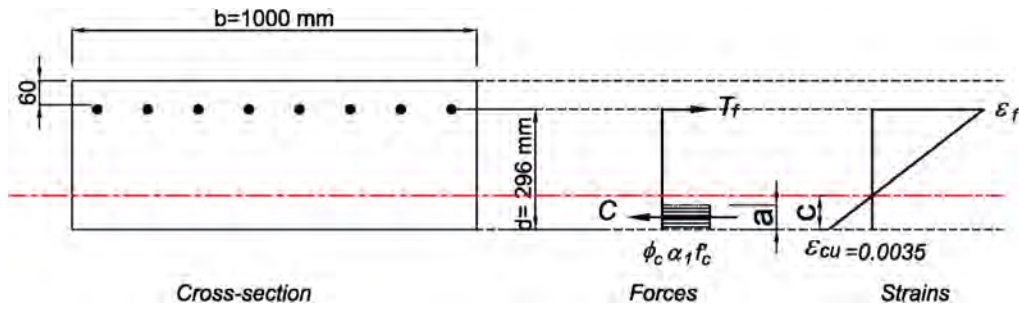


Fig. 16. Cross section of the slab at column locations

negative moment due to cracking and change in the flexural stiffness.

- The project's cost analysis confirmed that the initial higher cost of GFRP bars compared to steel does not necessarily lead to a higher total cost. The total cost of the GFRP-reinforced concrete slabs was almost the same (even less than) that of the steel-reinforced one. Replacing the asphalt layer with the polyurethane one made the difference in price between the GFRP and steel designs, thereby confirming that cost-effective designs could be achieved when the circumstances of the individual project are taken into consideration. About 40,000 linear meters of GFRP bars were used in this project.
- Finally, this successful field application demonstrated the use of GFRP reinforcing bars in a reinforced-concrete flat-slab parking garage. This first application of its type and scale, based on monitoring and continuous observations, performed structurally as anticipated. No major problems or any unexpected performance-associated difficulties occurred during construction or after 3.5 years under real service conditions. This application opens the door to major applications of FRP reinforcing bars in parking garages with extended service lives.

### Appendix. Typical Flexural Design Example—CSA S806-12 (CSA 2012)

This appendix provides a typical flexural design example according to the CSA (2012) *Design and Construction of Building Structures with Fibre Reinforced Polymers* for one section of the slab. The section is located in the column area where drop panels were provided. The total thickness of the slab at this section is 367 mm. The mechanical properties of the GFRP bars used in the design were provided in Table 2. This section was designed using GFRP bars of size #22 with a modulus of elasticity = 70.6 GPa

$$\text{Characteristic tensile strength} = \text{Average} - 3 \times \text{Standard Deviation} \quad (9a)$$

$$= 1,405 - 3 \times 37 = 1,294 \text{ MPa (corresponding strain} = 0.01832) \quad (9b)$$

From the structural analysis of the parking using SAFE Software (2011), the bending moments for one of the critical strips were (width of the strip = 4,267 mm)

$$M_f = 574.7 \text{ kN} \cdot \text{m}/\text{strip} = 134.7 \text{ kN} \cdot \text{m}/\text{m} \quad (10)$$

$$M_{\text{SLs}} = 436.0 \text{ kN} \cdot \text{m}/\text{strip} = 102.2 \text{ kN} \cdot \text{m}/\text{m} \quad (11)$$

The design for fire endurance necessitated a clear concrete cover of 60 mm. Fig. 16 shows the details of the cross-section

$$d = 367 - 60 - 22/2 = 296 \text{ mm} \quad (12)$$

Assume GFRP #22 at 140 mm ( $A_f = 2,764 \text{ mm}^2/\text{m}$ ), the material resistance for concrete and GFRP are denoted as

$$\phi_c = 0.65 \quad (13a)$$

$$\phi_f = 0.75 \quad (13b)$$

Stress block factors are

$$\begin{aligned} \alpha_1 &= 0.85 - 0.0015f'_c = 0.85 - 0.0015 \times (35) \\ &= 0.798 \geq 0.67 \text{ O.K} \end{aligned} \quad (14a)$$

$$\begin{aligned} \beta_1 &= 0.97 - 0.0025f'_c = 0.85 - 0.0025 \times (35) \\ &= 0.763 \geq 0.67 \text{ O.K} \end{aligned} \quad (14b)$$

$$a = \beta_1 c = 0.763c \quad (15)$$

and stress in concrete

$$\phi_c \alpha_1 f'_c = (0.65) \times (0.798) \times (35) = 18.2 \text{ MPa} \quad (16)$$

The strain in GFRP bars is

$$\frac{0.0035}{c} = \frac{\varepsilon_f}{d-c} \Rightarrow \varepsilon_f = \frac{0.0035}{c} (296 - c) \quad (17)$$

while the equilibrium of forces can be written as

$$C = \alpha_1 \phi_c f'_c b a = (18.2) \times (1,000) \times (0.763c) = 13,886.6c \quad (18)$$

$$\begin{aligned} T &= \phi_f \varepsilon_f E_f A_f = 0.75 \left[ \frac{0.0035}{c} (296 - c) \right] (70,600)(2,764) \\ &= \frac{151,622,536.8}{c} - 512,238.3 \end{aligned} \quad (19)$$

$$C = T \quad (20)$$

$$c^2 + 36.9c - 10,918.6 = 0 \quad (21a)$$

Solving for the neutral axis location

$$c = 87.6 \text{ mm} \quad (21b)$$

$$\begin{aligned} \frac{c}{d} &= \frac{87.6}{296} = 0.30 > \frac{7}{7 + 2,000\varepsilon_{fu}} \\ &= \frac{7}{7 + 2,000(0.01832)} = 0.16 \text{ O.K} \end{aligned} \quad (22)$$

the forces are

$$C = 13,886.6c = 1,216,466N \quad (23)$$

$$T = \frac{151,622,536.8}{c} - 512,238.3 = 1,218,613N \quad (24)$$

$$f_f = \frac{1,218,613}{2,764} = 441 \text{ MPa} \quad (25)$$

The resisting moment can be determined as

$$M_r = C \left( c - \frac{a}{2} \right) + T(d - c) \quad (26a)$$

$$\begin{aligned} M_r &= 1,216,466 \left( 87.6 - \frac{0.798 \times 87.6}{2} \right) \\ &+ 1,218,613(296 - 87.6) \end{aligned} \quad (26b)$$

$$M_r = 318.0 \times 10^6 \text{ N} \cdot \text{mm} > M_f (= 134.7 \times 10^6 \text{ N} \cdot \text{mm}) \text{ O.K} \quad (26c)$$

$$M_{cr} = f_r \frac{I_g}{y_t} = 0.6\sqrt{35} \frac{1,000(367)^3/12}{(367/2)} = 79.7 \times 10^6 \text{ N} \cdot \text{mm} \quad (27)$$

$$M_r > 1.5M_{cr} = 119.6 \times 10^6 \text{ N} \cdot \text{mm} \text{ O.K} \quad (28)$$

### Stress and Strain Limitations

The maximum stress in FRP bars under loads at serviceability limit state are denoted as

$$E_c = (3,000\sqrt{f'_c} + 6,900)(\gamma_c/2,300)^{1.5} = 26.27 \text{ GPa} \quad (29)$$

$$n = \frac{E_f}{E_c} = \frac{70.60}{26.27} = 2.69 \quad (30)$$

$$\rho = \frac{A_f}{bd} = \frac{2,764}{1,000 \times 296} = 0.00934 \quad (31)$$

$$k = \sqrt{(\rho n)^2 + 2\rho n} - \rho n = 0.2 \quad (32)$$

$$f_{fSLS} = \frac{M_{SLS}}{jdA_f} = \frac{M_{(D+L)}}{(1 - \frac{k}{3})dA_f} \quad (33a)$$

$$\begin{aligned} f_{fSLS} &= \frac{102.2 \times 10^6}{(1 - \frac{0.20}{3})(296)(2764)} = 133.8 \text{ MPa} < 0.25f_{fu} \\ &= 323.5 \text{ MPa O.K} \end{aligned} \quad (33b)$$

### Crack-Width Parameter Verification

$$\varepsilon_{fSLS} = \frac{f_{fSLS}}{E_f} = \frac{133.8}{70,600} = 0.0019 > 0.0015 \quad (34)$$

When the maximum strain in FRP tension reinforcement under full service loads exceeds 0.0015, the crack width parameter,  $z$ , should be verified

$$\text{Sand-coated GFRP bars, } k_b = 0.8 \quad (35)$$

$$d_c = h - d = 367 - 306 = 61 \text{ mm} \quad (36)$$

$$A = \frac{2d_c b}{n} = \frac{2(61)(1,000)}{7} = 17,428 \quad (37)$$

$$z = k_b \frac{E_s}{E_f} f_{fSLS} \sqrt[3]{d_c A} \quad (38a)$$

$$\begin{aligned} z &= 0.8 \times \frac{200,000}{70,600} (133.8) \sqrt[3]{(61)(17,428)} \\ &= 30,948 \text{ N/mm} < 38,000 \text{ N/mm O.K} \end{aligned} \quad (38b)$$

Note: In calculating  $d_c$  and  $A$ , the effective clear cover need not be taken as greater than 50 mm.

For the preceding, use GFRP#22 at 140 mm.

### Acknowledgments

The authors would like to thank and express their sincere appreciation to the Natural Science and Engineering Research Council of Canada (NSERC); the Canada Research Chair in Advanced Composite Materials for Civil Structures; and the NSERC/Industry Research Chair in Innovative FRP Reinforcement for Concrete Infrastructure in the Department of Civil Engineering, Faculty of Engineering, University of Sherbrooke (Sherbrooke, Quebec, Canada); the Fonds de recherche québécois en nature et technologies (FRQ-NT), and the City of Québec (parking-garage owner). The authors are also grateful to EMS Structure Inc. (consulting firm in Québec, Quebec, Canada), the general contractor Construction Paveton Inc., (Québec, Quebec, Canada); the GFRP reinforcement installer Les Ferrailleurs du Québec (Saint-Augustin-desmaures, Quebec, Canada); and the Department of Civil Engineering, University of Sherbrooke, for their technical support.

### Notation

The following symbols are used in this paper:

- $A$  = effective tensile area of concrete surrounding the flexural tensile reinforcement and extending from the extreme tensile fiber to the centroid of the flexural tensile reinforcement and an equal distance past the centroid, divided by the number of bars ( $\text{mm}^2$ );
- $A_b$  = area of an individual bar ( $\text{mm}^2$ );
- $A_f$  = area of FRP reinforcement ( $\text{mm}^2$ );

$A_g$  = gross area of section ( $\text{mm}^2$ );  
 $b_{o,0.5d}$  = critical perimeter at a distance of  $0.5d$  from the column face (mm);  
 $b_w$  = minimum effective web width (mm);  
 $C$  = compressive force resisted by the concrete above the neutral axis (kN);  
 $c$  = neutral-axis depth (mm);  
 $c_b$  = neutral-axis depth at the balanced strain condition (mm);  
 $d$  = effective depth (mm);  
 $d_b$  = bar diameter (mm);  
 $d_c$  = thickness of the cover from the tensile face to center of closest bar (mm);  
 $d_{cs}$  = distance from extreme tension fiber to the center of the longitudinal bar or wire located closest thereto (mm);  
 $d_v$  = effective shear depth, taken as the greater of  $0.90d$  or  $0.72h$ ;  
 $E_c$  = concrete modulus of elasticity (MPa);  
 $E_f$  = FRP modulus of elasticity (MPa);  
 $E_s$  = steel-reinforcement modulus of elasticity (MPa);  
 $f'_c$  = concrete compressive strength (MPa);  
 $f_{cr}$  = cracking strength of concrete (MPa);  
 $f_f$  = tensile stress in FRP reinforcement (MPa);  
 $f_{fSLS}$  = stress in the FRP reinforcement at service load level (MPa);  
 $f_{fu}$  = ultimate tensile strength of FRP (MPa);  
 $h_1$  = distance from neutral axis to center of tensile reinforcement (mm);  
 $h_2$  = distance from neutral axis to extreme tension fiber (mm);  
 $I_{cr}$  = transformed moment of inertia of cracked reinforced concrete section ( $\text{mm}^4$ );  
 $I_d$  = development length of FRP bars (mm);  
 $I_e$  = effective moment of inertia ( $\text{mm}^4$ );  
 $I_g$  = gross moment of inertia of uncracked section ( $\text{mm}^4$ );  
 $k_1$  = bar-location factor;  
 $k_2$  = concrete density factor;  
 $k_3$  = bar-size factor;  
 $k_4$  = bar-fiber factor;  
 $k_5$  = bar-surface profile factor;  
 $k_b$  = coefficient dependent on the reinforcing-bar bond characteristics;  
 $M_a$  = applied moment ( $\text{kN} \cdot \text{m}$ );  
 $M_{cr}$  = cracking moment of concrete ( $\text{kN} \cdot \text{m}$ );  
 $M_f$  = factored moment ( $\text{kN} \cdot \text{m}$ );  
 $M_r$  = factored moment resistance ( $\text{kN} \cdot \text{m}$ );  
 $M_{SLS}$  = moment at service limit state ( $\text{kN} \cdot \text{m}$ );  
 $n_f$  = ratio of modulus of elasticity of FRP bars to modulus of elasticity of concrete;  
 $s$  = bar spacing (mm);  
 $T$  = tension force resisted by the FRP reinforcement (kN);  
 $V_c$  = factored punching-shear resistance provided by the concrete (kN);  
 $W$  = maximum crack width (mm);  
 $z$  = crack-control parameter (N/mm);  
 $\alpha_1$  = ratio of average stress in the rectangular compression block to the specified concrete strength;  
 $\alpha_s$  = factor to adjust  $V_c$  for support dimensions: 4 for interior columns, 3 for edge columns, and 2 for corner columns;  
 $\beta_1$  = ratio of depth of equivalent rectangular stress block to depth of the neutral axis;  
 $\beta_c$  = the ratio of the column long side to short side, concentrated load, or reaction area;  
 $\gamma_c$  = density of concrete ( $\text{kN}/\text{m}^3$ );  
 $\varepsilon_c$  = maximum concrete compressive strain;  
 $\varepsilon_f$  = maximum tensile strain of FRP bars;

$\lambda$  = factor to account for concrete density;  
 $\rho_f$  = longitudinal FRP-reinforcement ratio;  
 $\phi_c$  = resistance factor for concrete; and  
 $\phi_f$  = resistance factor for FRP bars.

## References

- Ahmed, E., Dulude, C., and Benmokrane, B. (2011). "Construction and monitoring of the GFRP-reinforced flat slabs of the Hotel de Ville Parking Garage in Quebec City, Canada." *Technical Rep.*, City of Québec, Québec.
- Ahmed, E. A., Dulude, C., and Benmokrane, B. (2013a). "GFRP-reinforced concrete bridge barriers: Static tests and pendulum impacts." *Can. J. Civ. Eng.*, 40(11), 1050–1059.
- Ahmed, E. A., Matta, F., and Benmokrane, B. (2013b). "Steel post-and-beam barrier with FRP reinforced concrete curb and bridge deck connection." *J. Bridge Eng.*, 10.1061/(ASCE)BE.1943-5592.0000470, 1189–1197.
- Ahmed, E. A., Settecasì, F., and Benmokrane, B. (2014). "Construction and testing of steel-GFRP hybrid-reinforced-concrete bridge-deck slabs of the Ste-Catherine overpass bridges." *J. Bridge Eng.*, 10.1061/(ASCE)BE.1943-5592.0000581, 04014011.
- Benmokrane, B., El-Salakawy, E., El-Gamal, S., and Goulet, S. (2007). "Construction and testing of an innovative concrete bridge deck totally reinforced with glass FRP bars: Val-Alain Bridge on Highway 20 East." *J. Bridge Eng.*, 10.1061/(ASCE)1084-0702(2007)12:5(632), 632–645.
- Benmokrane, B., El-Salakawy, E., El-Ragaby, A., and Lackey, T. (2006). "Designing and testing of concrete bridge decks reinforced with glass FRP bars." *J. Bridge Eng.*, 10.1061/(ASCE)1084-0702(2006)11:2(217), 217–229.
- Benmokrane, B., El-Salakawy, E. F., Cherrak, Z., and Wiseman, A. (2004). "Fibre reinforced polymer composite bars for the structural concrete slabs of a Public Works and Government Service Canada parking garage." *Can. J. Civ. Eng.*, 31(5), 732–748.
- Bischoff, P. H., and Scanlon, A. (2007). "Effective moment of inertia for calculating deflections of concrete members containing steel reinforcement and FRP reinforcement." *ACI Struct. J.*, 104(1), 68–75.
- Canadian Consulting Engineer. (2008). "Fatal parking garage roof collapse in Montreal." (<http://www.canadianconsultingengineer.com/engineering/fatal-parking-garage-roof-collapse-in-montreal/1000087799/>) (Aug. 24, 2015).
- CSA (Canadian Standards Association). (2004). "Design of concrete structures for buildings." *CSA-A23.3 M-04*, Rexdale, ON, Canada.
- CSA (Canadian Standards Association). (2007). "Parking structures." *CAN/CSA 413-07*, Rexdale, ON, Canada.
- CSA (Canadian Standards Association). (2010). "Specification for fiber-reinforced polymers." *CAN/CSA S807-10*, Rexdale, ON, Canada.
- CSA (Canadian Standards Association). (2012). "Design and construction of building structures with fibre reinforced polymers." *CAN/CSA S806-12*, Rexdale, ON, Canada.
- De Luca, A., Matta, F., and Nanni, A. (2010). "Behavior of full-scale GFRP reinforced concrete columns under axial load." *ACI Struct. J.*, 107(5), 589–596.
- El-Mogy, M., El-Ragaby, A., and El-Salakawy, E. (2010). "Flexural behavior of continuous FRP-reinforced concrete beams." *J. Compos. Constr.*, 10.1061/(ASCE)CC.1943-5614.0000140, 669–680.
- El-Salakawy, E., Benmokrane, B., Masmoudi, R., Brière, F., and Breaumier, E. (2003). "Concrete bridge barriers reinforced with glass fiber-reinforced polymer composite bars." *ACI Struct. J.*, 100(6), 815–824.
- Hilti Canada. (2011). "HIT-HY 150 Max adhesive anchoring system." ([www.hilti.ca](http://www.hilti.ca)) (Apr. 12, 2015).
- Kodur, V. K. R., and Baingo, D. (1998). "Fire resistance of FRP-reinforced concrete slabs." *IR758*, National Research Council of Canada, Ottawa.
- Matta, F., and Nanni, A. (2009). "Connection of concrete railing post and bridge deck with internal FRP reinforcement." *J. Bridge Eng.*, 10.1061/(ASCE)1084-0702(2009)14:1(66), 66–76.
- Mufti, A., Bantia, N., Benmokrane, B., Boulfiza, M., and Newhook, J. (2007). "Durability of GFRP composite rods." *ACI Concr. Int.*, 29(2), 37–42.

- Nanni, A., and Faza, S. (2002). "Designing and constructing with FRP bars: An emerging technology." *ACI Concr. Int.*, 24(11), 53–58.
- NBCC (National Building Code of Canada). (2005). National Research Council, Ottawa.
- Pultrall. (2011). *FRP composite reinforcing rods*, Thetford Mines, Quebec.
- Razaqpur, A. G., Svecova, D., and Cheung, M. S. (1995). "Strength and deformations of FRP reinforced flat slab structures." *Proc., 2nd Int. RILEM Symp. (FRPRCS-2) Non-Metallic (FRP) Reinforcement for Concrete Structures*, L. Taerwe, ed., F & FN SPON, London, 322–329.
- SAFE Software. (2011). *Integrated design of flat slabs, foundation mats, and strip footings*, Computers and Structures, Walnut Creek, CA.